ACS SyntheticBiology

pubs.acs.org/synthbio

Technical Note

Cell-Free Expression of Soluble Leafhopper Proteins from Brochosomes

Caleb G. Lay, Gabriel R. Burks, Zheng Li, Jeffrey E. Barrick, Charles M. Schroeder, Ashty S. Karim, and Michael C. Jewett*

Cite This: *ACS Synth. Biol.* 2025, 14, 987−994

Read Online

ACCESS | Metrics & More | Article Recommendations | Supporting Information

ABSTRACT: Brochosomes are proteinaceous nanostructures produced by leafhopper insects with superhydrophobic and antireflective properties. Unfortunately, the production and study of brochosome-based materials has been limited by poor understanding of their major constituent subunit proteins, known as brochosomins, as well as their sensitivity to redox conditions due to essential disulfide bonds. Here, we used cell-free gene expression (CFE) to achieve recombinant production and analysis of brochosomin proteins. Through the optimization of redox environment, reaction temperature, and disulfide bond isomerase concentration, we achieved soluble brochosomin yields of up to 341 ± 30 μg/mL. Analysis using dynamic light scattering and transmission electron microscopy revealed distinct aggregation patterns among cell-free mixtures with different expressed brochosomins. We anticipate that the CFE methods developed here will accelerate the ability to change the geometries and properties of natural and modified brochosomes, as well as facilitate the expression and structural analysis of other poorly understood protein complexes.

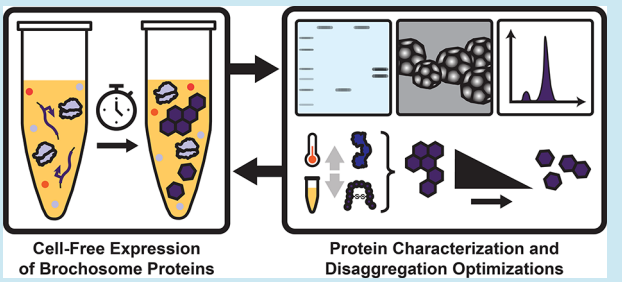

KEYWORDS: *Cell-free protein synthesis, brochosomes, disulfide bonds, self-assembly, protein folding, protein nanostructures*

INTRODUCTION

Nature provides a rich source of inspiration for the development of functional biomaterials. For example, spider silk contains C-terminal disulfide bonds that mediate fiber formation and enable its vaunted tensile properties used in many engineered materials.[1] Similarly, leafhoppers (family Cicadellidae) produce spherical disulfide-linked self-assembling protein nanostructures known as brochosomes that are typically 300−600 nm in size.[2] These structures coat the integument of adult leafhoppers, imparting superhydrophobic[3] and antireflective[4] properties hypothesized to protect the insects from fouling by their sticky honeydew[5] and/or to camouflage their bodies and, in some cases, their eggs.[3] These properties suggest potential applications for brochosomes in the development of synthetic materials including biocompatible antifouling coatings,[6] energy capture materials, and sensing devices.[4]

Despite their potential utility, brochosomes remain difficult to produce and study. Brochosomes appear to contain several structural protein subunits, the roles of which are not completely understood.[7] The major components are brochosomins, a family of proteins that exists in multiple copies in leafhopper genomes.[8] Brochosomes are highly sensitive to the redox environment; they are stable in neutral or oxidizing conditions but disassemble completely into their constituent subunits in reducing conditions due to disulfide bond cleavage.[7] The mechanisms behind full brochosome formation *in situ* are poorly understood but involve specialized cells in the Malpighian tubules of leafhoppers, in which brochosomes assemble and are excreted by Golgi-derived vacuoles with upregulated disulfide isomerase.[3,7] As a result of these challenges, prior studies have relied on harvesting brochosomes directly from leafhoppers or seeking to mimic them artificially using nonorganic bioinspired nanostructures.[4,9,10]

Cell-free gene expression (CFE) systems offer a promising platform for overcoming these challenges.[11] CFE enables the production of proteins in a modular and open reaction environment[12] conducive to rapid prototyping, allowing precise modulation of redox conditions, folding aids, and reaction components without concerns for cell viability.[13] CFE systems have been used previously to prototype numerous biochemical systems, including metabolism,[14−17] (poly)-peptide expression,[18−20] glycosylation,[21,22] biosensors,[23−27] and ribosomes,[28,29] as well as to create accessible education kits.[30−35] Of relevance to this study, CFE has been successfully

Received: November 6, 2024
Revised: February 3, 2025
Accepted: February 4, 2025
Published: March 7, 2025

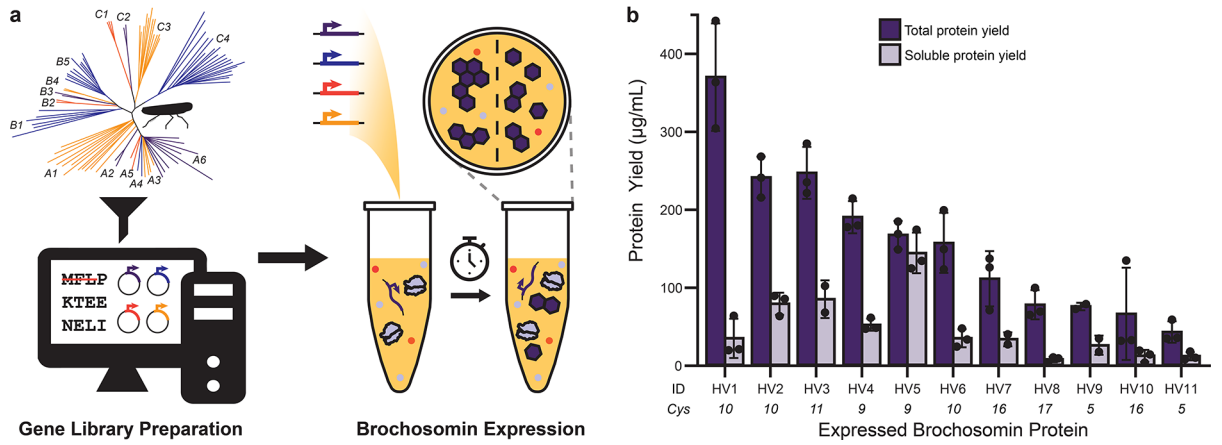

Figure 1. Brochosomin proteins were expressed in a bacterial CFE system. a. Overview of the process moving from analysis of brochosomin proteins in leafhopper transcriptomes to expression in *E. coli* cell-free lysate. During gene preparation, signal sequences were removed. **b.**Total and soluble protein yields in CFE show successful expression of *H. vitripennis* (HV) brochosomin proteins from linear expression templates (LETs). Soluble protein yields are generally low due to protein aggregation. The number of cysteine residues (Cys) for each protein is indicated below the protein ID. Error bars represent the average error of $n = 2$ or standard deviation of $n = 3$ replicates (individual data points shown).

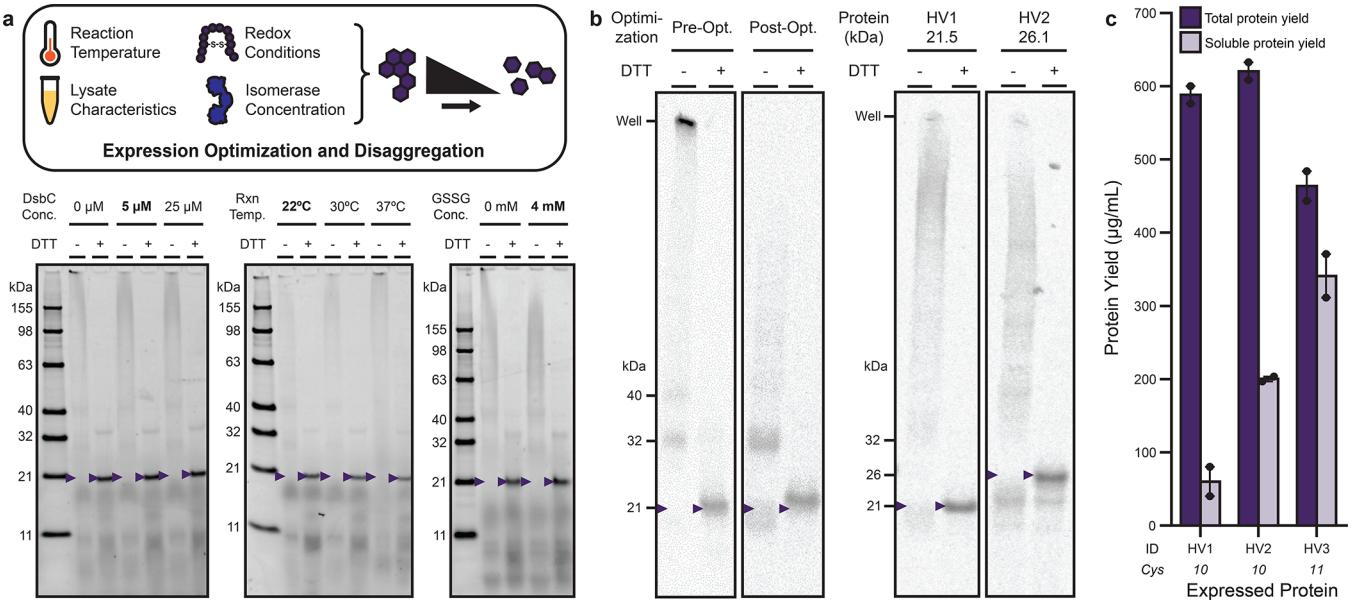

Figure 2. Optimization of CFE reaction conditions resulted in improved soluble expression of a brochosomin subset. a. Optimizations of CFE reactions were performed to reduce aggregation of brochosomin protein HV3. Nonreduced and reduced samples run in SDS-PAGE gels and imaged via fluorescence show minimal aggregation, as assessed by protein remaining in the well, at intermediate DsbC concentration, lowered reaction temperature, and with addition of oxidized glutathione. Bolded conditions were used for future reactions. **b.** HV3 (left gel) was expressed in pre- and post-optimization conditions using ^{14}C-leucine incorporation, run in SDS-PAGE gel, and developed as an autoradiogram. Disappearance of the large well-bound aggregates was observed, as well as darkening of bands at ∼21 and 32 kDa without DTT. These same optimizations, when applied to HV1 and HV2 (right gel), produced faint but significant banding at the expected size and reduced aggregation. Expected molecular weights are indicated with arrows. **c.** Total and soluble protein yields for the three brochosomin proteins show improvement over initial expression yields (Figure 1b), particularly for HV3. The number of cysteine residues (Cys) for each protein is indicated below the protein ID. Error bars represent the average error from $n = 2$ independent replicates.

used to produce various protein nanoparticles, including suckerin proteins,[36] virus-like particles[37−39] and ferritin nanocages,[40] which have been applied in vaccine development,[39,41] drug delivery,[39,41,42] and materials science.[36,43] These systems have demonstrated versatility in exploring protein self-assembly and structural formation under diverse conditions.

Brochosomes differ fundamentally from the protein nanostructures produced in prior studies in cell-free systems. They are significantly larger than typical virus-like particles (20−200 nm)[39] and ferritin cages (12 nm),[40] require precise conditions for folding of their disulfide-bonded subunit proteins, and have an unknown multimericity and composition.[7] Additionally, their *in vivo* assembly likely involves intricate eukaryotic cellular mechanisms that are difficult to replicate *in vitro*.[3,7] These unique properties present both a challenge and an opportunity for cell-free systems to explore and optimize synthesis and assembly of brochosome-like structures.

https://doi.org/10.1021/acssynbio.4c00773
ACS Synth. Biol. 2025, 14, 987−994

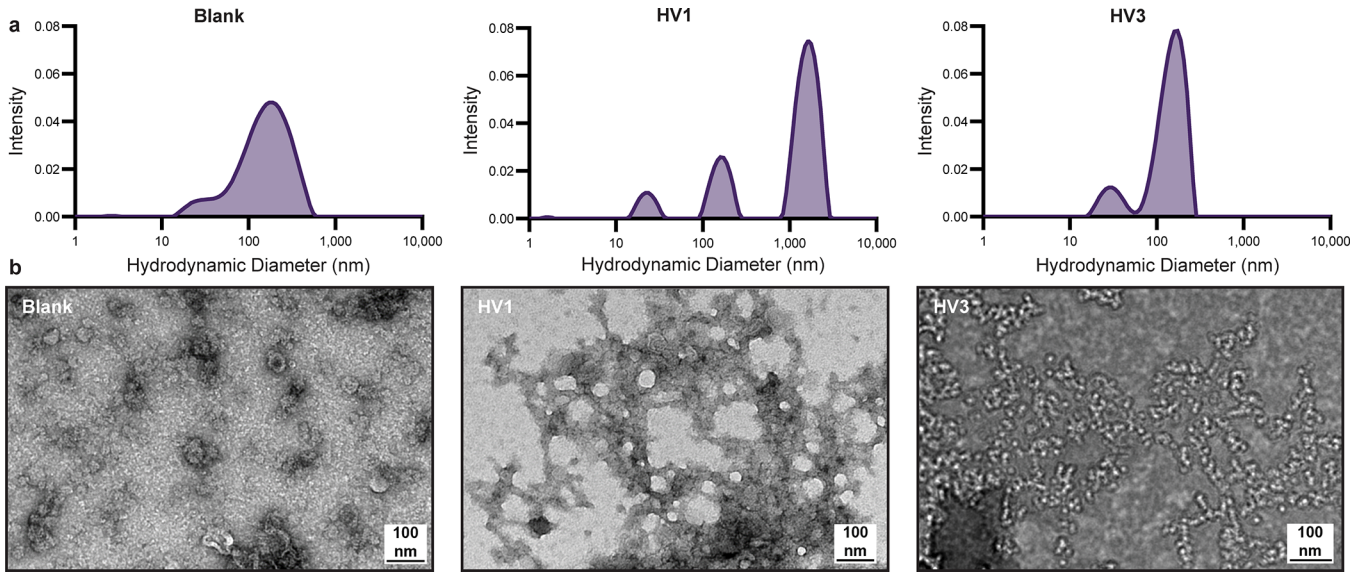

Figure 3. Optimization of CFE reaction conditions highlights differing aggregation behavior among brochosomins. a. DLS size distributions show peaks corresponding to ribosomes (~20 nm) and vesicles (~150 nm) in the blank sample (no recombinant protein expressed), with an additional ~1,000 nm peak appearing in HV1 samples, indicative of aggregation. HV3 samples lack this large peak, suggesting less aggregation under the same conditions. DLS curves represent the average of $n \geq 6$ technical replicates for each sample. **b.** Corresponding TEM images provide a visual comparison of these differences. The blank sample (left) shows relatively uniform features consistent with ribosomes and vesicles, while HV1 (middle) instead displays large, irregular aggregates. HV3 (right) shows more dispersed and smaller protein associations, consistent with reduced aggregation observed in DLS.

Here, we report the use of cell-free gene expression[44] as a platform to enable prototyping of brochosomin production and brochosome assembly conditions (Figure 1). In this work, we first expressed a large library of brochosomins in an *Escherichia coli*-based crude lysate CFE system. Next, we tuned disulfide bond isomerase concentration, reaction temperature, and redox conditions to improve soluble yield[12,45,46] and decrease brochosomin aggregation. Finally, we used dynamic light scattering (DLS) and transmission electron microscopy (TEM) to analyze brochosomin-enriched lysates to determine structural features (Supplementary Figure 1).

RESULTS AND DISCUSSION

Brochosomin Expression and Optimization in CFE. The overarching goal of this work was to use CFE to optimize production of brochosomes *in vitro*. To achieve this, we first designed codon-optimized DNA constructs for *E. coli* gene expression, removing native signal sequences. Although brochosome-related genes were identified and ordered from three leafhopper species (*Homalodisca vitripennis*, *Graphocephala fennahi*, and *Macrosteles quadrilineatus*), this study focused on brochosomin proteins from *H. vitripennis*. Eleven brochosomin proteins (HV1−HV11) were selected for study based on high-quality sequencing data and specific criteria designed to prioritize structurally integral brochosomins (see Methods). Constructs from *G. fennahi* and *M. quadrilineatus* were not tested, as the primary goal was to optimize expression and solubility for *H. vitripennis* brochosomins before expanding to other species.

H. vitripennis brochosomins were expressed in *E. coli*-based CFE reactions using the PANOx-SP system[47−49] in NEB SHuffle T7 Express-derived lysate, which is optimized for disulfide bond formation.[50] Reactions were incubated at 30 °C for 20 h, and soluble and total protein yields were quantified through radioactive ^{14}C-leucine incorporation.[51] Soluble yields ranged from 10−40% of total yields across all proteins tested (Figure 1b). Since the tested brochosomin proteins each contain 5 to 17 cysteine residues, we hypothesized that improper disulfide bond formation was causing insoluble aggregates to form in the non-native cell-free environment. SDS-PAGE analysis under reducing and nonreducing conditions supported this hypothesis, as proteins aggregated under nonreducing conditions but resolved to their expected molecular weights when reduced with dithiothreitol (DTT) (Supplementary Figure 2). These results suggest that aggregation is driven by disulfide bond misfolding and that further optimization of expression conditions could improve soluble yields and facilitate brochosomin assembly.

To better understand and optimize expression conditions, we focused on brochosomin protein HV3 because its banding pattern suggested minor formation of structured, soluble dimers. We hypothesized that the yield of soluble product could be increased by adjusting the concentration of supplemented *E. coli* disulfide bond isomerase DsbC, reaction temperature, and amount of oxidized glutathione (GSSG) added to the CFE reaction. We performed a series of optimizations for each of these factors using a range of values based on previous work with nonreducing CFE (GSSG: 0−4 mM; DsbC: 0−25 μM; Temperature: 22−37 °C) (Figure 2a). We found that a GSSG concentration of 4 mM, DsbC at 5 μM and a reaction temperature of 22 °C led to the best results at minimizing aggregated products. Combining each of these improvements led to a full disappearance of well-bound aggregates in the SDS-PAGE gel of HV3, as well as confirmation of soluble protein−protein interactions occurring (Figure 2b).

CFE Optimization Reduces Brochosomin Aggregate Formation. We next synthesized brochosomins HV1 and HV2 from *H. vitripennis* under optimized CFE conditions developed for HV3. While the ratio of total to soluble protein

https://doi.org/10.1021/acssynbio.4c00773
ACS Synth. Biol. 2025, 14, 987−994

did not change, the total and soluble yields of these two proteins improved after optimization (Figure 2c). We found that well-bound aggregates were reduced for each brochosomin compared to preoptimization conditions, though not to the same extent as HV3 (Figure 2b). Expression of HV2 also produced some unaggregated protein between 21 and 25 kDa in nonreducing conditions.

To better understand brochosomin aggregation, we measured size distributions of expressed proteins using dynamic light scattering (DLS). Our approach sought to characterize these aggregates without removing them from the lysate background to ensure that aggregates (or properly assembled structures) remained intact and were held in conditions representative of their expression. Analysis *in situ* is particularly important for brochosomins, which seem to require specific cellular features and physiochemical conditions to fold and assemble.[7] Thus, brochosomins HV1 and HV3 were expressed in optimized conditions via CFE, using a blank CFE reaction incubated without plasmid as a negative control. In our no plasmid control, two distinct peaks at 20 and 150 nm appear for ribosomes and inverted vesicles, respectively.[52] Measurements of HV1, which remained largely insoluble even with optimizations, revealed the appearance of distinct ∼1,000 nm particles which were not present in HV3 samples (Figure 3a).

We then visualized brochosomin aggregates via transmission electron microscopy (TEM). While intact harvested brochosomes have been imaged by TEM,[53] the appearance of their subunit intermediates is not well characterized. TEM images of our HV1 and HV3 samples (presented unpurified and in cell lysate) showed distinct aggregation profiles (Figure 3b). The large aggregates identified by DLS in HV1 appear to be visible as large, unstructured globular patches with sizes on the order of hundreds of nanometers that do not occur in our control sample. HV3, in comparison, had no such large aggregates, and some loose protein associations were observed in the sample. While these proteins were not confirmed as HV3, these semifilamentous associations were not observed elsewhere in HV1 or control samples. These results warrant further study of brochosomin expression and structure formation.

CONCLUSION

In this study, we demonstrated successful recombinant expression of soluble brochosomin proteins. Optimizations of disulfide bond isomerase addition, redox conditions, and reaction temperature improved the soluble expression of HV3, indicating that minor condition adjustments can have significant effects on brochosomin aggregation. Larger-scale combinatorial tuning of these conditions could similarly enable the soluble expression of all relevant subunit proteins. Additional strategies, such as vesicle[52] or nanodisc[54] enrichment to mimic native Golgi vacuoles or the addition of chaperone proteins, may further enhance proper folding and structure formation.

In addition, coexpressing combinations of these brochosomins together or with several brochosome-associated proteins (BSAPs) may be necessary for producing functional nanostructures.[7] BSAPs, which have poorly understood functions but are highly upregulated in brochosome-producing Malpighian tubule cells,[7,8] likely play key roles in brochosomin synthesis, folding, and/or assembly. Although full brochosome assembly was not attempted here, further optimization of soluble yields and post-expression purification could enable a mix-and-match approach for *in vitro* assembly. Similar strategies have been successfully applied to other self-assembling proteins, such as virus-like particles[55] and ferritin,[56] supporting the feasibility of this approach.

Overall, this study highlights the potential of cell-free systems not only for exploring brochosome assembly but also as a versatile platform for studying complex protein systems with diverse folding requirements.

METHODS

DNA Design and Preparation. Brochosomin-encoding sequences were identified in the transcriptomes and/or genomes of *Homalodisca vitrepennis*, *Graphocephala fennahi*, and *Macrosteles quadrilineatus* using iterative BLASTP searches with the protein sequences of candidate genes found in *G. fennahi* as the initial queries. For most of the *H. vitrepennis* sequences, the encoded proteins were found in purified brochosomes and the mRNAs and proteins were observed to be upregulated in the Malpighian tubules in a prior study.[7]

The SignalP signal peptide prediction tool was used to identify native signal sequences in both brochosomins.[8,57] Signal sequences with a peptide cleavage site prediction confidence greater than 95% were removed. Each resulting gene sequence was optimized for expression in *E. coli* using the Twist Bioscience optimization tool (Supplementary Table 1). Optimized sequences were synthesized and cloned into the pJL1 plasmid vector (AddGene Plasmid #69496) by Twist Bioscience. The constructs were provided both as purified plasmid DNA and as glycerol stocks in Twist Bioscience's proprietary *E. coli* cloning strain. Plasmid DNA was isolated using the ZymoPure II Plasmid Midiprep Kit (Zymo Research, Irvine, CA, USA), yielding concentrated DNA which was quantified using a Nanodrop 2000 Spectrophotometer (Thermo Fisher Scientific, Waltham, MA, USA) and subsequently diluted to a final concentration of 100 ng/μL.

Linear expression templates (LETs) were amplified from plasmid constructs using Q5 Hot Start High-Fidelity 2X Master Mix (New England Biolabs, Ipswich, MA, USA), following the manufacturer's protocol. An LET1 forward primer (CGATAAGTCGTGTCTTACCG) and reverse primer (GCATAAGCTTTTGCCATTCTC) were used for amplification, with annealing temperatures calculated using the NEB T_m calculator to ensure optimal primer binding conditions. The PCR conditions were as follows: initial denaturation at 98 °C for 30 s; 34 cycles of denaturation at 98 °C for 10 s, annealing at 62 °C for 20 s, and extension at 72 °C for 60 s; followed by a final extension at 72 °C for 2 min. The resulting PCR products were used directly as linear templates for subsequent cell-free expression reactions.

The selection of brochosomin proteins HV1−HV11 from *H. vitripennis* as the focus of the study followed several criteria. First, *H. vitripennis* was prioritized due to the availability of high-quality sequencing data; additional species were excluded to focus on first understanding assembly mechanisms within a single species. Second, nonbrochosomin proteins identified in the omics data were excluded, as their structural roles in brochosomes remain unclear. Proteins without detected stop codons were excluded to avoid fragments or incomplete sequences. Finally, proteins with signal sequences identified using SignalP were selected, as these sequences are consistent with secretion or processing in native brochosome production. These signal sequences were removed from ordered DNA constructs to facilitate recombinant expression in the *E. coli*

https://doi.org/10.1021/acssynbio.4c00773
ACS Synth. Biol. 2025, 14, 987−994

cell-free system. After applying these criteria, the only proteins that remained were HV1−HV11.

Cell Growth for Lysate Preparation. *E. coli* lysate was prepared using the Shuffle T7 Express strain (New England Biolabs, Ipswich, MA, USA), selected for its specific mutations that enhance disulfide bond reshuffling and promote proper protein folding. The cells were initially cultured in 50 mL of LB medium for 16 h. This starter culture was then used to inoculate 1 L of 2xYTP medium in a Tunair shake flask to a starting optical density at 600 nm (OD600) of 0.06. The culture was incubated at 37 °C with shaking at 220 rpm, and OD600 readings were taken every 20−30 min.

Once the culture reached an OD600 of 0.6, protein expression was induced by adding 500 μL of 1 M isopropyl β-D-1-thiogalactopyranoside (IPTG) to the medium. Growth continued until the cells reached an OD600 of 3.0. At this point, the culture was immediately transferred to a prechilled 1 L centrifuge bottle and centrifuged at 8000 × g for 5 min at 4 °C. The supernatant was discarded, and the cell pellet was divided between two 50 mL centrifuge tubes. Each tube received 25 mL of cold S30 buffer (10 mM Tris-acetate, 14 mM magnesium acetate, 60 mM potassium acetate). The cell pellets were resuspended using short bursts on a vortex mixer, with tubes kept on ice between bursts. Once fully resuspended, the cells were centrifuged again at 10,000 × g for 2 min at 4 °C. This wash step (resuspension, centrifugation, and supernatant removal) was repeated twice more. The final cell pellets were flash-frozen in centrifuge tubes using liquid nitrogen and stored at −80 °C until lysis.

Cell Lysate Preparation. Frozen cell pellets were thawed on ice for 1 h. For each centrifuge tube, 1 mL of S30 buffer was added per gram of cell pellet, and the pellets were resuspended using a vortex mixer in short bursts, with the cells kept on ice between mixing. The resuspended cells were loaded into a 20 mL syringe fitted with an 18-gauge needle and allowed to settle on ice for 10 min to dissipate bubbles. The syringe was then connected to an EmulsiFlex-B15 (Avestin, Ottawa, ON, Canada), and cell lysis was performed at approximately 22,000 psi.

The homogenized cell lysate was transferred to 1.5 mL microcentrifuge tubes and centrifuged at 12,000 × g for 10 min at 4 °C to remove insoluble debris. The clarified lysate, which appeared as a translucent amber supernatant, was carefully extracted, transferred to new microcentrifuge tubes, and centrifuged again. The clarified lysate from this step was consolidated and aliquoted. The aliquots were flash-frozen in liquid nitrogen and stored at −80 °C for subsequent use.

Cell-Free Expression Reaction. Cell-free gene expression was performed in 2 mL centrifuge tubes, using a 15 μL reaction mixture with the following components: 30% v/v S30 extract; 12 mM magnesium glutamate, 10 mM ammonium glutamate, and 130 mM potassium glutamate; 1.20 mM ATP and 0.85 mM each of CTP, GTP, and UTP; 340 mg/L folinic acid; 171 mg/L tRNA; 400 μM nicotinamide adenine dinucleotide (NAD); 0.27 mM coenzyme A; 4.0 mM oxalic acid; 1.0 mM putrescine; 1.5 mM spermidine; 57 mM HEPES; 2.0 mM of each standard amino acid; 30 mM phosphoenolpyruvate (PEP); 13.3 mg/L plasmid DNA or 2.00 μL linear DNA; and water to adjust to the final volume. Additionally, oxidized and reduced glutathione were included at specified ratios. Before being added to the reaction mixture, the S30 extract was treated with 1% v/v 50 mM iodoacetamide (IAM) for 30 min.

For fluorescence-based protein detection, 3.3% v/v FluoroTect GreenLys tRNA was included in the reaction. For protein quantification through autoradiography or protein analysis, ^{14}C-leucine was added to the mixture to a final concentration of 10 μM.

Fluorescence Gel Electrophoresis. Cell-free expression (CFE) reactions containing FluoroTect GreenLys tRNA were analyzed using fluorescence gel electrophoresis. A 4.5 μL aliquot of each reaction mixture was transferred to a PCR tube, treated with 1.5 μL of 4 mg/mL RNase A, and incubated at 37 °C for 10 min to reduce background. For reducing conditions, the treated sample was mixed with 3.75 μL LiCor loading buffer, 3.75 μL water, and 1.5 μL dithiothreitol (DTT). For nonreducing conditions, the mixture contained 3.75 μL LiCor loading buffer and 5.25 μL water. The mixture was then heated at 65 °C for 3 min and spun down to recover any evaporation.

Subsequently, 10 μL of the prepared sample was loaded onto a 4−12% Bis-Tris gel, along with 5 μL of Benchmark Fluorescent Ladder. The gel was run at 200 V for 40 min in 1X MES running buffer. After electrophoresis, the gel was carefully trimmed to remove nonessential regions and imaged using a LI-COR Odyssey Fc Imager (LI-COR Biosciences, Lincoln, NE, USA) with a 600 nm wavelength and 10 min exposure time. Contrast and brightness were adjusted as necessary using Image Studio software to enhance signal clarity.

Total and Soluble Protein Analysis. To quantify total and soluble protein, ^{14}C-leucine was added to each 15 μL cell-free expression (CFE) reaction at a final concentration of 10 μM. After a 20-h expression period, 5 μL of the reaction was mixed with 5 μL of 0.5 M potassium hydroxide (KOH) to assess total protein content. The remainder of the reaction was centrifuged at 16,000 × g for 10 min at 4 °C to separate soluble proteins. A 5 μL aliquot of the supernatant was then combined with 5 μL of 0.5 M KOH for soluble protein analysis.

For each KOH-denatured sample, 4 μL was spotted onto two glass fiber filtermats. One filtermat was washed three times with 4 °C trichloroacetic acid (TCA) to precipitate the proteins. Both filtermats were air-dried, then coated with melted scintillation wax. The radioactivity of the TCA-precipitated samples was quantified by solid scintillation counting (MicroBeta 2, PerkinElmer, Shelton, CT, USA). Protein yields were calculated using the counts from unwashed and TCA-washed filtermats, subtracting the background radiation measured from a negative control reaction lacking template DNA.

Protein Gel Autoradiography. Following 20 h of expression in reactions containing ^{14}C-leucine, 3 μL of each reaction was combined with 2.5 μL of LiCor 4x Protein Loading Buffer. For nonreduced samples, 4.5 μL of water was added; for reduced samples, 3.5 μL of water and 1 μL of 1 M dithiothreitol (DTT) were added. The samples were heated at 65 °C for 3 min to minimally disrupt structural disulfide bonds.

Next, 5 μL of each sample was loaded onto a 4−12% bis-tris gel and electrophoresed at 120 V for 40 min using MES running buffer. After electrophoresis, the gel was stained with Coomassie blue for 30 min. The stained gel was then placed between two moistened cellophane sheets and vacuum-dried for 2 h at 60 °C.

The dried gel was placed in a cartridge with a phosphoscreen, which was exposed for 3−5 days. The phosphoscreen was scanned using a 650 nm laser (Typhoon

https://doi.org/10.1021/acssynbio.4c00773
ACS Synth. Biol. 2025, 14, 987−994

FLA 7000, Cytiva Life Sciences, Marlborough, MA, USA), and the resulting autoradiogram was aligned with a visible-light gel image to determine band intensities and assess protein expression.

Dynamic Light Scattering Analysis. For particle size analysis, 5 μL of each cell-free expression (CFE) reaction was gently transferred by pipet into a BladeCell disposable sample cuvette. The cuvette was then loaded into a NanoDLS pUNK system (Unchained Laboratories, Pleasanton, CA, USA) for dynamic light scattering measurement.

Each sample underwent six 20-s measurements, which were averaged to produce a correlation function. Particle size distributions were then calculated using the system's proprietary regularization algorithm (RADLS). This algorithm reconstructs smooth, continuous size distributions by resolving multimodal populations and complies with ISO 22412:2017 standards for particle size analysis.

To preserve native aggregation states and physiochemical conditions, samples were measured directly without purification. Particle sizes were calculated using a model with bovine serum albumin (BSA) as the buffer standard and globular proteins as the reference for molecular weight estimation. The combined data from the measurements provided size distributions for assessing the protein aggregation state in each sample.

Microscopy Analysis. Sample imaging was conducted on a Thermo Fisher FEI Tecnai G2 F20 S-TWIN STEM at 120 kV. Prior to imaging, 4 μL of brochosomin solution was drop cast onto a carbon coated TEM grid, allowed to settle for 1 min, wicked of excess solvent, and subsequently stained using a uranyl acetate heavy metal staining procedure. The STEM and sample preparation facilities were utilized at the University of Illinois at Urbana−Champaign Beckman Institute for Advanced Sciences.

■ ASSOCIATED CONTENT

Data Availability Statement

All data are presented in the paper and Supporting Information. Source data is available upon request.

Supporting Information

The Supporting Information is available free of charge at https://pubs.acs.org/doi/10.1021/acssynbio.4c00773.

> Figures showing a detailed workflow and demonstrating of gel images of HV1−HV11 in unoptimized conditions; table with amino acid sequences of HV1−HV11 (PDF)

■ AUTHOR INFORMATION

Corresponding Author

Michael C. Jewett − *Department of Chemical and Biological Engineering and Center for Synthetic Biology, Northwestern University, Evanston, Illinois 60208, United States; Department of Bioengineering, Stanford University, Stanford, California 94305, United States;* orcid.org/0000-0003-2948-6211; Email: mjewett@stanford.edu

Authors

Caleb G. Lay − *Department of Chemical and Biological Engineering and Center for Synthetic Biology, Northwestern University, Evanston, Illinois 60208, United States;* orcid.org/0009-0006-1916-3346

Gabriel R. Burks − *Department of Chemical and Biomolecular Engineering, University of Notre Dame, Notre Dame, Indiana 46556, United States;* orcid.org/0000-0003-0985-0450

Zheng Li − *Department of Integrative Biology, The University of Texas at Austin, Austin, Texas 78712, United States*

Jeffrey E. Barrick − *Department of Molecular Biosciences, Center for Systems and Synthetic Biology, The University of Texas at Austin, Austin, Texas 78712, United States;* orcid.org/0000-0003-0888-7358

Charles M. Schroeder − *Department of Materials Science and Engineering, University of Illinois Urbana−Champaign, Urbana, Illinois 61801, United States;* orcid.org/0000-0001-6023-2274

Ashty S. Karim − *Department of Chemical and Biological Engineering and Center for Synthetic Biology, Northwestern University, Evanston, Illinois 60208, United States;* orcid.org/0000-0002-5789-7715

Complete contact information is available at: https://pubs.acs.org/10.1021/acssynbio.4c00773

Author Contributions

C.G.L. and M.C.J. designed the study. J.E.B. and Z.L. provided protein sequences and omics data and aided experiment design. C.G.L. performed all cell-free expression experiments and all nonmicroscopy analysis. G.R.B. performed all microscopy imaging. M.C.J., J.E.B., and C.M.H. supervised the research. C.G.L., M.C.J., and A.S.K. wrote the manuscript. All authors edited and reviewed the manuscript.

Notes

The authors declare no competing financial interest.

■ ACKNOWLEDGMENTS

C.G.L. thanks Kosuke Seki, Andrew Hunt, and Maddie DeWinter for guidance on disulfide-bonded protein expression and Grant Rybnicky for DLS training. We thank Nancy Moran for input on the design of the study. We acknowledge the Army Research Office for funding (W911NF-20-1-0195, W911NF-22-2-0246, W911NF-23-1-0334).

■ REFERENCES

(1) Grip, S.; Johansson, J.; Hedhammar, M. Engineered disulfides improve mechanical properties of recombinant spider silk. *Protein Sci.* **2009**, *18* (5), 1012−1022.

(2) Rakitov, R. A. Powdering of egg nests with brochosomes and related sexual dimorphism in leafhoppers (Hemiptera: Cicadellidae). *Zoological Journal of the Linnean Society* **2004**, *140* (3), 353−381.

(3) Rakitov, R.; Gorb, S. N. Brochosomal coats turn leafhopper (Insecta, Hemiptera, Cicadellidae) integument to superhydrophobic state. *Proceedings of the Royal Society B: Biological Sciences* **2013**, *280* (1752), No. 20122391.

(4) Yang, S.; Sun, N.; Stogin, B. B.; Wang, J.; Huang, Y.; Wong, T.-S. Ultra-antireflective synthetic brochosomes. *Nat. Commun.* **2017**, *8*, 1.

(5) Rakitov, R.; Gorb, S. N. Brochosomes protect leafhoppers (Insecta, Hemiptera, Cicadellidae) from sticky exudates. *Journal of The Royal Society Interface* **2013**, *10* (87), No. 20130445.

(6) Ghaffari, S.; Aliofkhazraei, M.; Barati Darband, G.; Zakeri, A.; Ahmadi, E. Review of superoleophobic surfaces: Evaluation, fabrication methods, and industrial applications. *Surfaces and Interfaces* **2019**, *17*, No. 100340.

(7) Rakitov, R.; Moysa, A. A.; Kopylov, A. T.; Moshkovskii, S. A.; Peters, R. S.; Meusemann, K.; Misof, B.; Dietrich, C. H.; Johnson, K. P.; Podsiadlowski, L.; Walden, K. K. O. Brochosomins and other novel proteins from brochosomes of leafhoppers (Insecta, Hemiptera, Cicadellidae). *Insect Biochem. Mol. Biol.* **2018**, *94*, 10−17.

(8) Li, Z.; Li, Y.; Xue, A. Z.; Dang, V.; Holmes, V. R.; Johnston, J. S.; Barrick, J. E.; Moran, N. A. The Genomic Basis of Evolutionary Novelties in a Leafhopper. *Mol. Biol. Evol.* **2022**, *39* (9), msac184.
(9) Si, Y.; Huang, T.; Xie, H.; Chen, M. Synthesis of Biomimetic Brochosome-Shaped Microspheres via Droplets Assembly Strategy. *Chem. Mater.* **2022**, *34* (16), 7271−7279.
(10) Jakšić, Z.; Obradov, M.; Jakšić, O. Brochosome-Inspired Metal-Containing Particles as Biomimetic Building Blocks for Nanoplasmonics: Conceptual Generalizations. *Biomimetics* **2021**, *6* (4), 69.
(11) Hunt, A. C.; Rasor, B. J.; Seki, K.; Ekas, H. M.; Warfel, K. F.; Karim, A. S.; Jewett, M. C. Cell-Free Gene Expression: Methods and Applications. *Chem. Rev.* **2025**, *125* (1), 91−149.
(12) Carlson, E. D.; Gan, R.; Hodgman, C. E.; Jewett, M. C. Cell-free protein synthesis: Applications come of age. *Biotechnology Advances* **2012**, *30* (5), 1185−1194.
(13) Batista, A. C.; Soudier, P.; Kushwaha, M.; Faulon, J. L. Optimising protein synthesis in cell-free systems, a review. *Engineering Biology* **2021**, *5* (1), 10−19.
(14) Vögeli, B.; Schulz, L.; Garg, S.; Tarasava, K.; Clomburg, J. M.; Lee, S. H.; Gonnot, A.; Moully, E. H.; Kimmel, B. R.; Tran, L. Cell-free prototyping enables implementation of optimized reverse β-oxidation pathways in heterotrophic and autotrophic bacteria. *Nat. Commun.* **2022**, *13* (1), 3058.
(15) Liew, F. E.; Nogle, R.; Abdalla, T.; Rasor, B. J.; Canter, C.; Jensen, R. O.; Wang, L.; Strutz, J.; Chirania, P.; De Tissera, S.; et al. Carbon-negative production of acetone and isopropanol by gas fermentation at industrial pilot scale. *Nat. Biotechnol.* **2022**, *40* (3), 335−344.
(16) Karim, A. S.; Dudley, Q. M.; Juminaga, A.; Yuan, Y.; Crowe, S. A.; Heggestad, J. T.; Garg, S.; Abdalla, T.; Grubbe, W. S.; Rasor, B. J.; et al. In vitro prototyping and rapid optimization of biosynthetic enzymes for cell design. *Nat. Chem. Biol.* **2020**, *16* (8), 912−919.
(17) Karim, A. S.; Jewett, M. C. A cell-free framework for rapid biosynthetic pathway prototyping and enzyme discovery. *Metabolic engineering.* **2016**, *36*, 116−126.
(18) Landwehr, G. M.; Bogart, J. W.; Magalhaes, C.; Hammarlund, E. G.; Karim, A. S.; Jewett, M. C. Accelerated enzyme engineering by machine-learning guided cell-free expression. *bioRxiv* **2024**, 2024.2007.2030.605672.
(19) Liu, W.-Q.; Ji, X.; Ba, F.; Zhang, Y.; Xu, H.; Huang, S.; Zheng, X.; Liu, Y.; Ling, S.; Jewett, M. C. Cell-free biosynthesis and engineering of ribosomally synthesized lanthipeptides. *Nat. Commun.* **2024**, *15* (1), 4336.
(20) Hunt, A. C.; Vögeli, B.; Hassan, A. O.; Guerrero, L.; Kightlinger, W.; Yoesep, D. J.; Krüger, A.; Dewinter, M.; Diamond, M. S.; Karim, A. S. A rapid cell-free expression and screening platform for antibody discovery. *Nat. Commun.* **2023**, *14* (1), 3897.
(21) Stark, J. C.; Jaroentomeechai, T.; Moeller, T. D.; Hershewe, J. M.; Warfel, K. F.; Moricz, B. S.; Martini, A. M.; Dubner, R. S.; Hsu, K. J.; Stevenson, T. C.; et al. On-demand biomanufacturing of protective conjugate vaccines. *Science Advances* **2021**, *7* (6), No. eabe9444.
(22) Kightlinger, W.; Duncker, K. E.; Ramesh, A.; Thames, A. H.; Natarajan, A.; Stark, J. C.; Yang, A.; Lin, L.; Mrksich, M.; Delisa, M. P. A cell-free biosynthesis platform for modular construction of protein glycosylation pathways. *Nat. Commun.* **2019**, *10* (1), 5404.
(23) Thavarajah, W.; Silverman, A. D.; Verosloff, M. S.; Kelley-Loughnane, N.; Jewett, M. C.; Lucks, J. B. Point-of-Use Detection of Environmental Fluoride via a Cell-Free Riboswitch-Based Biosensor. *ACS Synth. Biol.* **2020**, *9* (1), 10−18.
(24) Ekas, H. M.; Wang, B.; Silverman, A. D.; Lucks, J. B.; Karim, A. S.; Jewett, M. C. Engineering a PbrR-Based Biosensor for Cell-Free Detection of Lead at the Legal Limit. *ACS Synth. Biol.* **2024**, *13* (9), 3003−3012.
(25) Silverman, A. D.; Akova, U.; Alam, K. K.; Jewett, M. C.; Lucks, J. B. Design and Optimization of a Cell-Free Atrazine Biosensor. *ACS Synth. Biol.* **2020**, *9* (3), 671−677.
(26) Jung, J. K.; Archuleta, C. M.; Alam, K. K.; Lucks, J. B. Programming cell-free biosensors with DNA strand displacement circuits. *Nat. Chem. Biol.* **2022**, *18* (4), 385−393.
(27) Pardee, K.; Green, A. A.; Ferrante, T.; Cameron, D. E.; DaleyKeyser, A.; Yin, P.; Collins, J. J. Paper-Based Synthetic Gene Networks. *Cell* **2014**, *159* (4), 940−954.
(28) Kofman, C.; Willi, J. A.; Karim, A. S.; Jewett, M. C. Ribosome Pool Engineering Increases Protein Biosynthesis Yields. *ACS Central Science* **2024**, *10*, 871−881.
(29) Krüger, A.; Watkins, A. M.; Wellington-Oguri, R.; Romano, J.; Kofman, C.; Defoe, A.; Kim, Y.; Anderson-Lee, J.; Fisker, E.; Townley, J. Community science designed ribosomes with beneficial phenotypes. *Nat. Commun.* **2023**, *14* (1), 961.
(30) Stark, J. C.; Huang, A.; Nguyen, P. Q.; Dubner, R. S.; Hsu, K. J.; Ferrante, T. C.; Anderson, M.; Kanapskyte, A.; Mucha, Q.; Packett, J. S.; et al. BioBits Bright: A fluorescent synthetic biology education kit. *Science Advances* **2018**, *4* (8), No. eaat5107.
(31) Huang, A.; Nguyen, P. Q.; Stark, J. C.; Takahashi, M. K.; Donghia, N.; Ferrante, T.; Dy, A. J.; Hsu, K. J.; Dubner, R. S.; Pardee, K.; et al. BioBits Explorer: A modular synthetic biology education kit. *Science Advances* **2018**, *4* (8), No. eaat5105.
(32) Collins, M.; Lau, M. B.; Ma, W.; Shen, A.; Wang, B.; Cai, S.; La Russa, M.; Jewett, M. C.; Qi, L. S. A frugal CRISPR kit for equitable and accessible education in gene editing and synthetic biology. *Nat. Commun.* **2024**, *15* (1), 6563.
(33) Jung, J. K.; Rasor, B. J.; Rybnicky, G. A.; Silverman, A. D.; Standeven, J.; Kuhn, R.; Granito, T.; Ekas, H. M.; Wang, B. M.; Karim, A. S.; et al. At-Home, Cell-Free Synthetic Biology Education Modules for Transcriptional Regulation and Environmental Water Quality Monitoring. *ACS Synth. Biol.* **2023**, *12* (10), 2909−2921.
(34) Rybnicky, G. A.; Dixon, R. A.; Kuhn, R. M.; Karim, A. S.; Jewett, M. C. Development of a Freeze-Dried CRISPR-Cas12 Sensor for Detecting *Wolbachia* in the Secondary Science Classroom. *ACS Synth. Biol.* **2022**, *11* (2), 835−842.
(35) Collias, D.; Marshall, R.; Collins, S. P.; Beisel, C. L.; Noireaux, V. An educational module to explore CRISPR technologies with a cell-free transcription-translation system. *Synthetic Biology* **2019**, *4* (1), ysz005.
(36) Hershewe, J. M.; Wiseman, W. D.; Kath, J. E.; Buck, C. C.; Gupta, M. K.; Dennis, P. B.; Naik, R. R.; Jewett, M. C. Characterizing and Controlling Nanoscale Self-Assembly of Suckerin-12. *ACS Synth. Biol.* **2020**, *9* (12), 3388−3399.
(37) Bundy, B. C.; Franciszkowicz, M. J.; Swartz, J. R. Escherichia coli-based cell-free synthesis of virus-like particles. *Biotechnol. Bioeng.* **2008**, *100* (1), 28−37.
(38) Wang, X.; Liu, J.; Zheng, Y.; Li, J.; Wang, H.; Zhou, Y.; Qi, M.; Yu, H.; Tang, W.; Zhao, W. M. An optimized yeast cell-free system: Sufficient for translation of human papillomavirus 58 L1 mRNA and assembly of virus-like particles. *J. Biosci. Bioeng.* **2008**, *106* (1), 8−15.
(39) Nooraei, S.; Bahrulolum, H.; Hoseini, Z. S.; Katalani, C.; Hajizade, A.; Easton, A. J.; Ahmadian, G. Virus-like particles: preparation, immunogenicity and their roles as nanovaccines and drug nanocarriers. *J. Nanobiotechnol.* **2021**, *19* (1), 59.
(40) Contreras-Llano, L. E.; Meyer, C.; Liu, Y.; Sarker, M.; Lim, S.; Longo, M. L.; Tan, C. Holistic engineering of cell-free systems through proteome-reprogramming synthetic circuits. *Nat. Commun.* **2020**, *11* (1), 3138.
(41) Rodríguez-Limas, W. A.; Sekar, K.; Tyo, K. E. J. Virus-like particles: the future of microbial factories and cell-free systems as platforms for vaccine development. *Curr. Opin. Biotechnol.* **2013**, *24* (6), 1089−1093.
(42) Ikwuagwu, B.; Tullman-Ercek, D. Virus-like particles for drug delivery: a review of methods and applications. *Curr. Opin. Biotechnol.* **2022**, *78*, No. 102785.
(43) Uchida, M.; Klem, M. T.; Allen, M.; Suci, P.; Flenniken, M.; Gillitzer, E.; Varpness, Z.; Liepold, L. O.; Young, M.; Douglas, T. Biological Containers: Protein Cages as Multifunctional Nanoplatforms. *Adv. Mater.* **2007**, *19* (8), 1025−1042.
(44) Silverman, A. D.; Karim, A. S.; Jewett, M. C. Cell-free gene expression: an expanded repertoire of applications. *Nat. Rev. Genet.* **2020**, *21* (3), 151−170.

https://doi.org/10.1021/acssynbio.4c00773
ACS Synth. Biol. 2025, 14, 987−994

(45) Garenne, D.; Haines, M. C.; Romantseva, E. F.; Freemont, P.; Strychalski, E. A.; Noireaux, V. Cell-free gene expression. *Nature Reviews Methods Primers* **2021**, *1* (1), 49.
(46) Dondapati, S. K.; Stech, M.; Zemella, A.; Kubick, S. Cell-Free Protein Synthesis: A Promising Option for Future Drug Development. *BioDrugs* **2020**, *34* (3), 327−348.
(47) Jewett, M. C.; Swartz, J. R. Mimicking the *Escherichia coli* cytoplasmic environment activates long-lived and efficient cell-free protein synthesis. *Biotechnol. Bioeng.* **2004**, *86* (1), 19−26.
(48) Jewett, M. C.; Calhoun, K. A.; Voloshin, A.; Wuu, J. J.; Swartz, J. R. An integrated cell-free metabolic platform for protein production and synthetic biology. *Molecular Systems Biology* **2008**, *4* (1), 220.
(49) Kwon, Y.-C.; Jewett, M. C. High-throughput preparation methods of crude extract for robust cell-free protein synthesis. *Sci. Rep.* **2015**, *5* (1), 8663.
(50) Mohammadi, E.; Seyedhosseini-Ghaheh, H.; Mahnam, K.; Jahanian-Najafabadi, A.; Sadeghi Mir Mohammad, H. Reteplase: Structure, Function, and Production. *Advanced Biomedical Research* **2019**, *8* (1), 19.
(51) Martin, R. W.; Des Soye, B. J.; Kwon, Y.-C.; Kay, J.; Davis, R. G.; Thomas, P. M.; Majewska, N. I.; Chen, C. X.; Marcum, R. D.; Weiss, M. G. Cell-free protein synthesis from genomically recoded bacteria enables multisite incorporation of noncanonical amino acids. *Nat. Commun.* **2018**, *9* (1), 1203.
(52) Hershewe, J. M.; Warfel, K. F.; Iyer, S. M.; Peruzzi, J. A.; Sullivan, C. J.; Roth, E. W.; Delisa, M. P.; Kamat, N. P.; Jewett, M. C. Improving cell-free glycoprotein synthesis by characterizing and enriching native membrane vesicles. *Nat. Commun.* **2021**, *12* (1), 2363.
(53) Burks, G. R.; Yao, L.; Kalutantirige, F. C.; Gray, K. J.; Bello, E.; Rajagopalan, S.; Bialik, S. B.; Barrick, J. E.; Alleyne, M.; Chen, Q.; et al. Electron Tomography and Machine Learning for Understanding the Highly Ordered Structure of Leafhopper Brochosomes. *Biomacromolecules.* **2023**, *24* (1), 190−200.
(54) Koo, C. W.; Hershewe, J. M.; Jewett, M. C.; Rosenzweig, A. C. Cell-Free Protein Synthesis of Particulate Methane Monooxygenase into Nanodiscs. *ACS Synth. Biol.* **2022**, *11* (12), 4009−4017.
(55) Le, D. T.; Müller, K. M. In Vitro Assembly of Virus-Like Particles and Their Applications. *Life* **2021**, *11* (4), 334.
(56) Wang, C.; Liu, Q.; Huang, X.; Zhuang, J. Ferritin nanocages: a versatile platform for nanozyme design. *J. Mater. Chem. B* **2023**, *11* (19), 4153−4170.
(57) Teufel, F.; Almagro Armenteros, J. J.; Johansen, A. R.; Gíslason, M. H.; Pihl, S. I.; Tsirigos, K. D.; Winther, O.; Brunak, S.; Von Heijne, G.; Nielsen, H. SignalP 6.0 predicts all five types of signal peptides using protein language models. *Nat. Biotechnol.* **2022**, *40* (7), 1023−1025.

https://doi.org/10.1021/acssynbio.4c00773
ACS Synth. Biol. 2025, 14, 987−994